Role of electron transfer in Ce^{3+} sensitized Yb^{3+} luminescence in borate glass

Atul D. Sontakke,[1,a)] Jumpei Ueda,[1,2] Yumiko Katayama,[1] Yixi Zhuang,[1] Pieter Dorenbos,[2] and Setsuhisa Tanabe[1]
[1]*Graduate School of Human and Environmental Studies, Kyoto University, Kyoto 606-8501, Japan*
[2]*Delft University of Technology, Faculty of Applied Science, Department of Radiation Science and Technology (FAME-LMR), 2629 JB Delft, The Netherlands*

(Received 5 October 2014; accepted 19 December 2014; published online 5 January 2015)

In a Ce^{3+}-Yb^{3+} system, two mechanisms are proposed so far namely, the quantum cutting mechanism and the electron transfer mechanism explaining Yb^{3+} infrared luminescence under Ce^{3+} excitation. Among them, the quantum cutting mechanism, where one Ce^{3+} photon (ultraviolet/blue) gives rise to two Yb^{3+} photons (near infrared) is widely sought for because of its huge potential in enhancing the solar cell efficiency. In present study on Ce^{3+}-Yb^{3+} codoped borate glasses, Ce^{3+} sensitized Yb^{3+} luminescence at $\sim$1 μm have been observed on Ce^{3+} 5d state excitation. However, the intensity of sensitized Yb^{3+} luminescence is found to be very weak compared to the strong quenching occurred in Ce^{3+} luminescence in Yb^{3+} codoped glasses. Moreover, the absolute luminescence quantum yield also showed a decreasing trend with Yb^{3+} codoping in the glasses. The overall behavior of the luminescence properties and the quantum yield is strongly contradicting with the quantum cutting phenomenon. The results are attributed to the energetically favorable electron transfer interactions followed by Ce^{3+}-$Yb^{3+} \rightleftharpoons Ce^{4+}$-$Yb^{2+}$ inter-valence charge transfer and successfully explained using the absolute electron binding energies of dopant ions in the studied borate glass. Finally, an attempt has been presented to generalize the electron transfer mechanism among opposite oxidation/reduction property dopant ions using the vacuum referred electron binding energy (VRBE) scheme for lanthanide series. © *2015 AIP Publishing LLC*. [http://dx.doi.org/10.1063/1.4905317]

I. INTRODUCTION

Recent advancements in solar cell photovoltaic (PV) have shown huge interest in the development of efficient luminescent solar concentrators (LSCs). Several dyes, quantum dots and rare earth lanthanides activated optical materials are widely investigated for LSC application.[1–3] Among them, the rare earth ions have gained special attention owing to their high luminescence quantum yield and the ability for quantum cutting mechanism (cooperative energy transfer based down-conversion), which shows great potential to overcome the Shockley-Queisser limit of 29% in case of *c*-Si PV cells.[4,5] In quantum cutting, the active ions absorb high energy photons and convert them into two or more low energy photons. Many rare earth ions including Eu^{3+},[6] Gd^{3+}-Eu^{3+},[6] Pr^{3+},[7] Er^{3+}-Tb^{3+},[8] Pr^{3+}-Yb^{3+},[9] Tm^{3+}-Yb^{3+},[10] Tb^{3+}-Yb^{3+},[11] etc., have shown the cooperative down-conversion from UV to visible or visible to near infrared region.

The quantum cutting process is useful to increase the absolute photon counts at the PV band gap region.[12] Also it can reduce the thermalization losses occurring due to the absorption of excess energy photons above PV band gap. The rare earth ions exhibiting broad absorption profile in ultraviolet (UV) to blue spectral region are proposed to be advantageous so that a wider spectral region can be utilized for the quantum cutting process. Ce^{3+}-Yb^{3+},[5] Eu^{2+}-Yb^{3+},[13] Tb^{3+}-Yb^{3+},[11] and Pr^{3+}-Yb^{3+}(Ref. 9) are some of the interesting dopant pairs studied in this regard. Among them, the Ce^{3+}-Yb^{3+} pair has extensively been investigated in recent years because of the wideband absorption profile of Ce^{3+} ions in the UV-blue spectral region, high luminescence quantum yield of both Ce^{3+} and Yb^{3+} ions, and the strong Ce^{3+}-Yb^{3+} inter-ionic interactions.[5,14–17] In a Ce^{3+}-Yb^{3+} codoped system, Ce^{3+} 4f $\rightarrow$ 5d excitation gives rise to Yb^{3+} $^2F_{5/2} \rightarrow {}^2F_{7/2}$ emission at $\sim$1 μm.[5] Since there are no intermediate resonant energy levels between Ce^{3+} and Yb^{3+} ions, and the Ce^{3+} emission photons ($5d_1 \rightarrow 4f$) are almost twice the energy of Yb^{3+} infrared photons; Ce^{3+} sensitization to Yb^{3+} ions is primarily attributed to the quantum cutting mechanism. Several reports have proposed efficient quantum cutting in Ce^{3+}-Yb^{3+} codoped materials with theoretical quantum yield reaching close to 200% as estimated from the donor (Ce^{3+}) luminescence decay lifetime and energy transfer efficiency values.[14–16] To substantiate such high quantum yield, Ueda and Tanabe experimentally (integrating sphere method) investigated the absolute quantum yield of Ce^{3+}-Yb^{3+} luminescence in $Y_3Al_5O_{12}$ ceramic.[5] They observed that the Yb^{3+} codoping indeed acts as a strong deactivator for Ce^{3+} luminescence and gives rise to Yb^{3+} emission; however, the absolute quantum yield of the system also decreases. The effect was attributed to the presence of inter-valence charge transfer (IVCT) based electron transfer mechanism among Ce^{3+}-Yb^{3+} ions ($Ce^{3+} + Yb^{3+} \rightleftharpoons Ce^{4+} + Yb^{2+}$) instead of the

a)E-mail: sontakke.atul.55a@st.kyoto-u.ac.jp

quantum cutting mechanism. Setlur and Shiang further studied the electron transfer mechanism in Ce^{3+}-Yb^{3+}/Eu^{3+} codoped $Y_3Al_5O_{12}$ and $Lu_2Si_2O_7$ hosts, and proposed a semi-classical thermodynamic approach to estimate the thermal activation energies for electron transfer.[18] The results were found to be consistent with the experimental data. In addition to this, the electron trapping character of Yb^{3+} ($Yb^{3+} + e^- \rightarrow Yb^{2+}$) ions in Ce^{3+}-Yb^{3+} codoped $Y_3Al_5O_{12}$ ceramic has been studied by You *et al*. using thermoluminescence (TL) spectroscopy and corresponding quenching mechanism has been discussed.[19] According to all these studies, the electron transfer mechanism is primarily responsible for the quenching of Ce^{3+} luminescence in presence of Yb^{3+} ions instead of the quantum cutting mechanism.

In view of the rare earth energy level structure, it seems convincing that the electron transfer mechanism is dominant in almost all of the Ce^{3+}-Yb^{3+} codoped host materials. However, there are some recent reports especially in glassy hosts claiming the presence of efficient quantum cutting mechanism.[14–16] Another report on a transparent glass-ceramic host suggests the presence of multi-phonon assisted single photon energy transfer mechanism among Ce^{3+}-Yb^{3+} dopant pairs.[17] Since the electron transfer mechanism has experimentally been established in Ce^{3+}-Yb^{3+} codoped $Y_3Al_5O_{12}$ ceramic, it is interesting to investigate whether the similar mechanism is present in glassy hosts. [5,18,19] Therefore, in the present investigation, Ce^{3+}-Yb^{3+} codoped borate glasses have been prepared and studied for their photoluminescence (PL), luminescence quantum yield and PL decay lifetime properties. Special attention has been given to precisely obtain the experimental luminescence quantum yield since it is decisive in understanding the overall photon yield in singly and codoped samples. Moreover, the electron transfer or the IVCT mechanism requires a detailed knowledge of energy level position of the Ce^{3+} $5d_1$ state (donor) and the Yb^{2+} ground state (acceptor) in the host band structure.[19] The host referred as well as the vacuum referred electron binding energy diagrams of Ce^{3+} and Yb^{3+} ions have been constructed for the present borate glasses and the corresponding mechanism is discussed in detail.

II. EXPERIMENTAL METHODS

The glass samples in the present investigation with base composition of 55 B_2O_3 – 20 CaO – 10 Al_2O_3 – 15 La_2O_3 (in mol. %) were prepared using the high temperature melt-quenching method. The doped samples were obtained by partially substituting the La^{3+} contents with the Ce^{3+} and Yb^{3+} contents, respectively. CeF_3 and Yb_2O_3 were used as precursor chemicals for the dopant ions and the melting was carried out in presence of excess carbon (0.5 wt. %) to achieve cerium in trivalent state. For both dopants, an equivalent amount of La_2O_3 (0.5 mol. % in case of Ce^{3+}; and 1, 3, and 5 mol. % in case of Yb^{3+}) was substituted by the respective chemicals. The well-mixed ingredients were melted in covered high-purity alumina crucibles at 1350 °C for 45 min. For reducing atmosphere, each crucible was surrounded by carbon powder enclosed in a bigger crucible. The melt was then quenched on a warm stainless steel mold. The cast glasses were annealed at 600 °C for stress removal and cooled slowly to the room temperature. The well-annealed glasses were cut and polished in $10 \times 10 \times 2\,mm^3$ dimensions for various measurements. All the glasses were named according to their dopant contents.

Optical absorption spectra were recorded using a Shimadzu 3600 spectrophotometer in the wavelength range of 180–1200 nm and 2500–3200 nm, respectively. To avoid the saturation effect due to the strong absorption in the UV region, thin samples (~200 μm thickness) were used for optical absorption studies. The longer wavelength region spectra were recorded to investigate the OH^- presence in the studied borate glass. The spectra showed a broad absorption profile peaking at around 2800 nm with absorption coefficient (α_{OH}) of about 3 cm^{-1}. The host phonon energy of the studied glass was investigated using Fourier Transform Infrared (FTIR) spectroscopy (Shimadzu, FTIR8400s) and was found to be about 1350 cm^{-1}. Photoluminescence (PL) spectra of the studied glasses were obtained in the range of 380–1200 nm by pumping with a 372 nm laser diode (LD) (Nichia Co. Ltd., NDHU110APAE3) excitation. The PL signals were collected using a 90 mm focal length quartz lens, which were then dispersed using a monochromator (Nikon, G250) and recorded using a Si photodiode detector (Electro-Optical System Inc., S-025-H). All the PL spectra were calibrated using a standard halogen lamp (Labsphere, SCL-600). PL excitation (PLE) spectra for Ce^{3+} and Yb^{3+} luminescence were recorded using a 300 W Xe lamp (Max 302, Asahi Spectra) as an excitation source together with a monochromator (Nikon, G250) and Si photodiode detector. A standard Si photodiode (Spectroscopic Instruments, SI337-1010BQ) was used for signal calibration. The PL quantum yield was measured using a 10 inch integrating sphere (Labsphere Inc., LMS-100) attached with multi-channel CCD detectors (Ocean Optics Inc., USB 2000 and USB2000+) and 372 nm LD. Signals were calibrated using a standard halogen lamp (Labsphere, SCL-600) and an auxiliary halogen lamp for absolute spectral distribution and absorption losses, respectively. The PL decay curves were recorded using a PL lifetime measurement setup (Hamamatsu-Photonics, Quantarus Tau) equipped with a picosecond LED (temporal resolution ~ 0.5 ns) for Ce^{3+} decay measurement and a Xenon flash lamp (temporal resolution ~ 10 μs) for Yb^{3+} decay measurement, respectively.

III. RESULTS

A. Ce^{3+} and Yb^{3+} absorption profile in borate glass

Figure 1 presents the optical absorption spectra of the base glass and the Ce^{3+}, Yb^{3+} singly doped glasses. From the base glass absorption spectrum, it is clear that the present borate glass exhibits wide ultraviolet (UV) transmission with the fundamental optical absorption edge starting at around 200 nm. This is advantageous in the present study, since both Ce^{3+} and Yb^{3+} ions exhibit characteristic absorption transitions in the UV spectral region.[19] In the Ce^{3+} singly doped glass, intense 4f → 5d absorption transitions of Ce^{3+} ions are observed between 200 and 380 nm. In the base glass corrected absorption profile, five distinct components could be

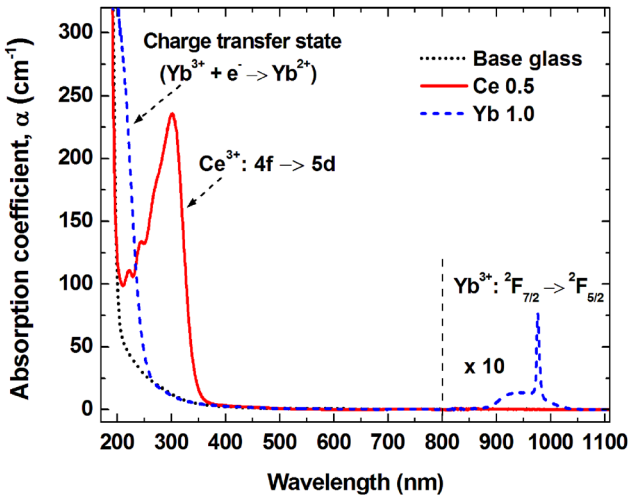

FIG. 1. Optical absorption spectra of base glass, Ce^{3+} singly doped and Yb^{3+} singly doped glass samples. (Sample thickness ~ 200 μm).

observed, suggesting a distorted symmetry of Ce^{3+} ions in the studied borate glass. In case of Yb^{3+} doped glass, two absorption transitions have been observed. The high energy transition at around 250 nm is attributed to the $Yb^{3+} + e^{-} \rightarrow Yb^{2+}$ charge transfer state (CTS); whereas the absorption at around 980 nm is due to the Yb^{3+} f – f transition ($^2F_{7/2} \rightarrow {}^2F_{5/2}$). The absorption coefficient of Yb^{3+} f – f transition appears significantly weaker compared to its CTS transition or the Ce^{3+} 4f → 5d transitions.

B. Photoluminescence, excitation, and luminescence quantum yield

Figure 2 shows the PL spectra of Ce^{3+} singly and Ce^{3+}-Yb^{3+} codoped glasses under 372 nm LD excitation. The 372 nm excitation was used to avoid the direct Yb^{3+} excitation via CTS as well as to restrict the Ce^{3+} ionization to the conduction band. In singly doped glass, Ce^{3+} shows a broad luminescence centered at 450 nm due to the $5d_1 \rightarrow 4f$ electronic transitions. On Yb^{3+} codoping, the intensity of Ce^{3+} luminescence exhibits strong quenching and the Yb^{3+} luminescence appears at 980 nm due to the $^2F_{5/2} \rightarrow {}^2F_{7/2}$ transition. The sensitized Yb^{3+} luminescence first increases from 1 to 3 mol% Yb_2O_3 concentration and then decreases for higher concentration. It can be seen that the intensity of Yb^{3+} luminescence is very weak in view of the strong quenching of Ce^{3+} luminescence in the codoped glasses. Figure 3 shows the excitation spectra of the studied glasses monitoring the Yb^{3+} luminescence at 980 nm. In the Ce^{3+}-Yb^{3+} codoped glasses, the spectra reveal a broad excitation profile composed of Ce^{3+}: 4f → 5d transitions and the Yb^{3+} CTS transition as assigned in the figure. The excitation spectra of Yb^{3+} singly doped glass has also been presented in Figure 3 showing the Yb^{3+} CT transition. In the codoped glasses, the Yb^{3+} CT transition is dominant at shorter wavelength region (<280 nm), whereas the Ce^{3+} 4f → 5d transitions are stronger at longer wavelength region. The presence of Ce^{3+} 4f → 5d transitions in the excitation spectrum of Yb^{3+} emission substantiates the Ce^{3+} sensitization to the Yb^{3+} luminescence in studied glasses. The excitation profile intensity also follows the similar trend as the Yb^{3+} luminescence intensity attaining a maximum for 3 mol. % Yb_2O_3 codoping and then decreases for higher Yb_2O_3 concentration. This decrease in the Yb^{3+} luminescence and the excitation intensity at higher Yb_2O_3 concentration is due to the migration assisted quenching process which becomes prominent with the increase in dopant concentration. Similar trend has been observed in the Yb^{3+} decay lifetime. The Yb^{3+} decay lifetime is 772 μs in 1 mol. % Yb_2O_3 and 767 μs in 3 mol. % Yb_2O_3 codoped glass and then decreases to 420 μs in the 5 mol. % Yb_2O_3 codoped glass.

In order to obtain more quantitative information about the luminescence properties, the luminescence quantum yield of singly and codoped glasses was measured using an integrating sphere. Figure 4 presents the absolute luminescence quantum yield (η) of both Ce^{3+} and Yb^{3+} luminescence as a function of Yb_2O_3 concentration in the studied glasses. The integrated PL intensity histogram of Ce^{3+} and Yb^{3+} luminescence is also presented in the figure. For Ce^{3+} singly doped glass, the luminescence quantum yield is found to be about 42%. On Yb_2O_3 codoping, the quantum yield

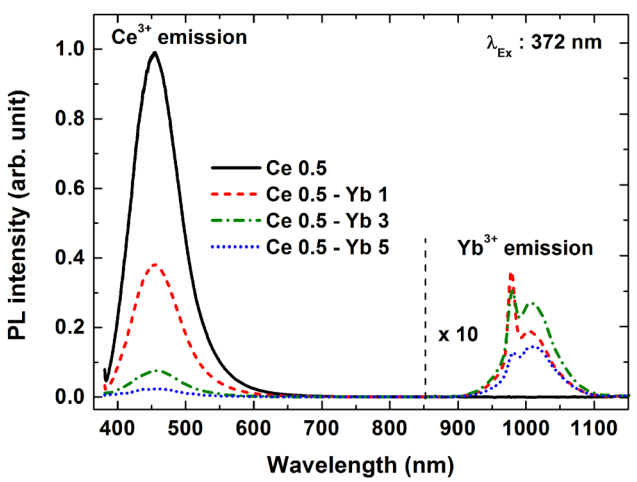

FIG. 2. PL spectra of Ce^{3+} singly and Ce^{3+}-Yb^{3+} codoped glasses under Ce^{3+} excitation at 372 nm.

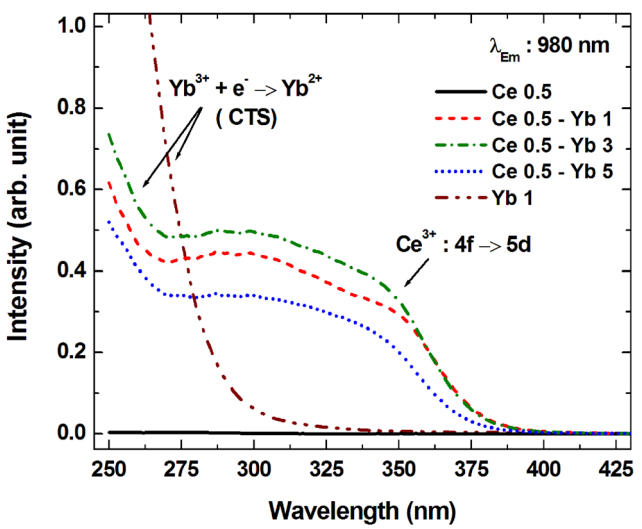

FIG. 3. PL excitation spectra of Ce^{3+} singly doped, Yb^{3+} singly doped and Ce^{3+}-Yb^{3+} codoped glasses monitoring Yb^{3+} infrared emission at 980 nm.

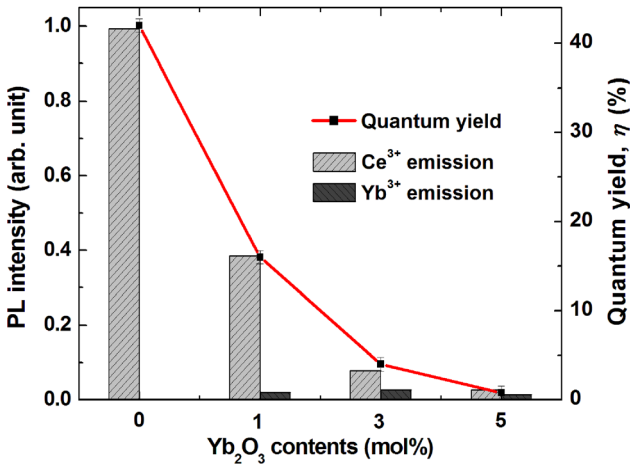

FIG. 4. PL intensity histogram and absolute quantum yield as a function of Yb_2O_3 concentration.

exhibits strong quenching and decreases from 42% in Ce^{3+} singly doped glass to about 16% in 1 mol. % Yb_2O_3 codoped glass and less than 1% in 5 mol. % Yb_2O_3 codoped glass.

C. Ce^{3+} luminescence decay lifetime and energy transfer efficiency

Figure 5 shows the PL decay curves monitoring Ce^{3+} emission at 450 nm under 340 nm excitation. For Ce^{3+} singly doped glass, the decay curve is nearly single exponential with decay lifetime of about 46 ns. However, it becomes non-exponential in the codoped glasses and exhibits faster decay. Figure 6 shows the plot of the Ce^{3+} PL decay lifetime (τ) and the $Ce^{3+} \rightarrow Yb^{3+}$ energy transfer efficiency (η_{ET}) as a function of the Yb_2O_3 concentration. The decay lifetime and energy transfer efficiency values were obtained using the standard expressions.[20] The decay lifetime shows a continuous decrease from about 46 ns in the Ce^{3+} singly doped glass to about 11 ns for the 5 mol. % Yb_2O_3 codoped glass, giving rise to an energy transfer efficiency of 76%.

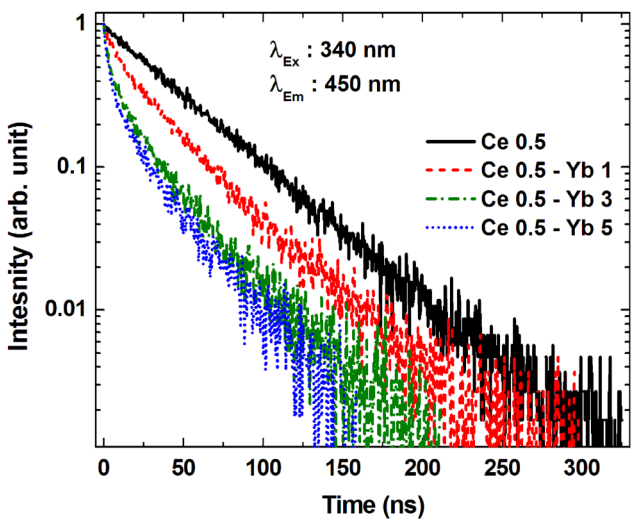

FIG. 5. Ce^{3+} PL decay curves in Ce^{3+} singly and Ce^{3+}-Yb^{3+} codoped glasses.

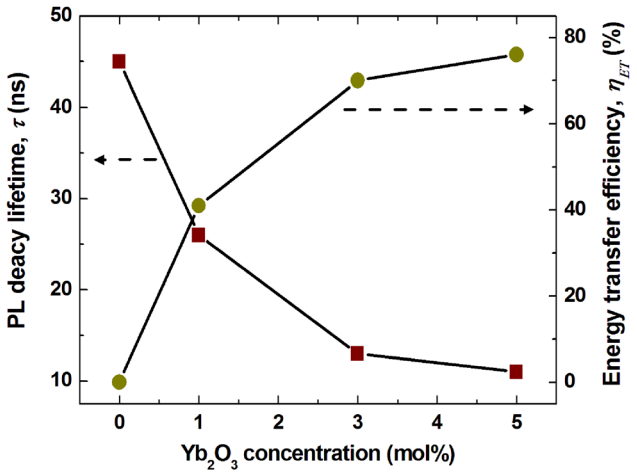

FIG. 6. Ce^{3+} PL decay lifetime and $Ce^{3+} \rightarrow Yb^{3+}$ energy transfer efficiency as a function of Yb_2O_3 concentration.

IV. DISCUSSION

It is clear from the photoluminescence and lifetime results that the Yb^{3+} ions cause strong quenching in the Ce^{3+} luminescence. In the literature, this is often attributed to the quantum cutting mechanism, where one Ce^{3+} photon gives rise to two Yb^{3+} photons in the infrared region (Ce^{3+}:$5d_1 \rightarrow 4f \Rightarrow 2Yb^{3+}$:$^2F_{7/2} \rightarrow {}^2F_{5/2}$).[14–16] This is reasonable in view of the energy level structure of Ce^{3+} and Yb^{3+} ions, which are completely non-resonant for the direct energy transfer from Ce^{3+} to Yb^{3+} ions. In the quantum cutting mechanism, the absolute quantum yield of the system should increase, since each high energy photon (Ce^{3+}) generates two low energy photons (Yb^{3+}). But the experimental results in the present study clearly shows a decrease in absolute quantum yield value in the codoped glasses. This behavior strongly contradicts with the quantum cutting phenomenon.[6,12] Moreover, the quantum cutting is a cooperative energy transfer mechanisms, which is very weak and exists only in densely codoped materials.[21] In our case, Ce^{3+} luminescence decreases by more than half of its magnitude for a mere 1 mol. % Yb_2O_3 codoping. Similar results were obtained in $Y_3Al_5O_{12}$ ceramic.[5,18] Setlur and Shiang suggested that such high quenching rate is possible only by an electron transfer interaction, where the transfer rate is significantly greater than the typical energy transfer rate for non-radiative electrostatic interactions.[18]

A. Host referred electron binding energies of Ce^{3+} and Yb^{3+} ions

In order to understand the electron transfer mechanism, the host referred electron binding energy (HRBE) diagram of Ce^{3+} and Yb^{3+} ions has been constructed and presented in Figure 7. The electron binding energies of the dopant ions are estimated from the observed energy for charge (electron) transfer ($Ce^{4+} + e^- \rightarrow Ce^{3+}$ and $Yb^{3+} + e^- \rightarrow Yb^{2+}$), Ce^{3+}: $4f \rightarrow 5d$ absorption, Yb^{3+}: $^2F_{7/2} \rightarrow {}^2F_{5/2}$ absorption, and the fundamental absorption band of the host glass.[22] The charge transfer energy helps in locating the lanthanide ground state level with respect to the top of the valence band. The energy

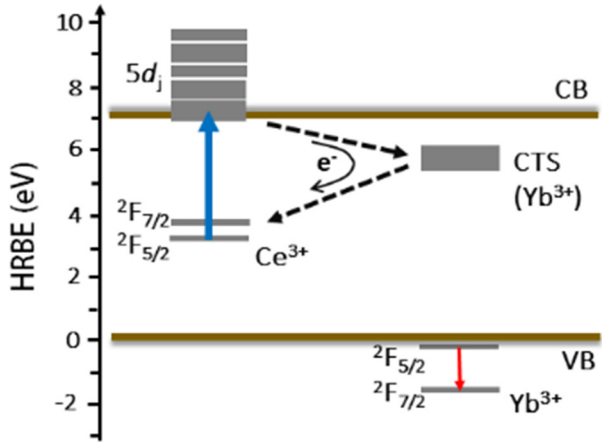

FIG. 7. Host referred electron binding energies of Ce^{3+} and Yb^{3+} ions in borate glass. The electron transfer path is represented by dashed lines.

of charge transfer, E^{CT} of a lanthanide ion (Ln^n) from the valence band provides the 4f ground state energy of its $(n+1)$ configuration. Figure 8 shows the absorption profiles of the Ce^{3+}: 4f → 5d transitions and the charge transfer transitions of Ce^{4+}, Yb^{3+} and the Eu^{3+} ions in the studied borate glass. In order to obtain the Ce^{4+} and Eu^{3+} CT, the corresponding glasses were prepared in the oxidizing condition. The charge transfer transitions exhibit high absorption coefficients and therefore only the onset of transitions could be obtained for some ions. In general, the Eu^{3+} CT energy is used to estimate the 4f ground state energy of Eu^{2+}, and then the energies for other lanthanide ions are calculated.[22–24] In case of Ce^{4+}, the onset of CT agrees well in establishing the Ce^{3+} ground state energy with respect to the top of the host valence band. Accordingly, the Ce^{3+} ground state energy is estimated to be 3.3 ± 0.1 eV and the corresponding 5d excited states were constructed using the 4f → $5d_j$ absorption transition energies. The Yb^{2+} ground state energy is estimated to be 5.9 ± 0.2 eV from the CT transition. In order to locate the position of the conduction band, the optical bandgap energy was first calculated from the UV absorption

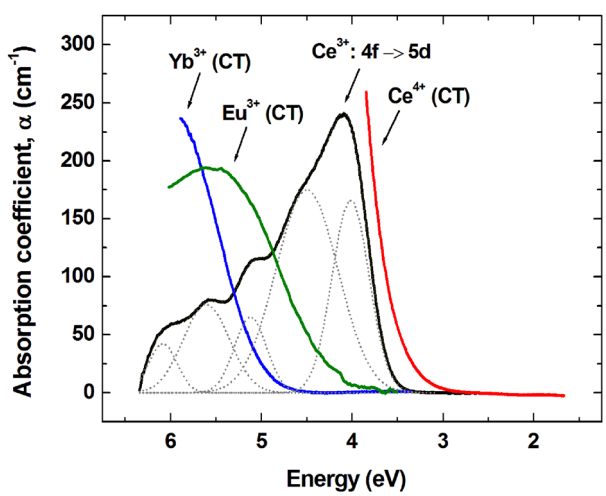

FIG. 8. Base glass corrected absorption profiles of Ce^{3+} 4f → $5d_j$ transitions and Ce^{4+}, Eu^{3+}, and Yb^{3+} charge transfer transitions. (Dotted lines represent the deconvoluted components of Ce^{3+} absorption).

profile. It was found to be 6.3 ± 0.1 eV for the studied borate glass. In case of crystalline hosts, it has been suggested to consider the valence to conduction band energy about 8–10% higher than the optical bandgap energy while constructing the HRBE diagram in order to compensate the contribution due to the near-edge defect centers as well as the temperature influence.[22,23] Similar treatment has been assumed in the construction of HRBE diagram for present borate glass. Accordingly, the conduction band is placed at 7 ± 0.2 eV above the valence band in the HRBE diagram.

From the Figure 7, it can be seen that the excited $5d_1$ state of the Ce^{3+} ions is located at the same energy as that of the bottom of the conduction band, whereas the higher $5d_j$ levels are inside the conduction band. This is in accordance with the results on the temperature dependent decay lifetime study of the present Ce^{3+} singly doped borate glass. The results reveal a low (~60 meV) activation energy for the thermally stimulated ionization process from Ce^{3+} $5d_1$ state to the conduction band. Such a small value of thermal activation energy substantiates that the $5d_1$ excited state is very close to the bottom of the conduction band.[25] The Ce^{3+} excitation spectra in Figure 3 also support this observation. The peak position of the Ce^{3+} excitation profile exhibits a red shift compared to the corresponding absorption profile suggesting the quenching of higher energy excitation levels due to their proximity to the conduction band.

B. $Ce^{3+} \rightarrow Yb^{3+}$ electron transfer mechanism

From the HRBE diagram in Figure 7, it is clear that the lowest $5d_1$ component of Ce^{3+} is at higher energy than the Yb^{2+} ground state suggesting that the electron transfer from Ce^{3+} (5d) to Yb^{3+} is energetically favorable. Accordingly, the electrons excited to the Ce^{3+} $5d_1$ state are transferred to the neighboring Yb^{3+} ions creating Ce^{4+}-Yb^{2+} pairs. This electron transfer may take place via different processes such as the quantum tunneling, orbital overlapping or through the conduction band.[19] In case of the $Y_3Al_5O_{12}$ ceramics, You *et al.* have suggested that the Ce^{3+} to Yb^{3+} electron transfer is more likely to occur through the spectral overlap of the Ce^{3+} 5d orbital with the 4f orbital of nearest-neighboring Yb^{3+} ions.[19] The newly formed Ce^{4+}-Yb^{2+} pair is energetically less stable compared to the Ce^{3+}(4f)-Yb^{3+} pair; and therefore, the electron tries to back transfer to the Ce^{3+} ground state.[19,26] Since the Yb^{2+} ground state is at lower energy than the Ce^{3+}: $5d_1$ state, the electron can only go to the Ce^{3+} ground states as depicted in Fig. 7. In this process, Yb^{3+} may return in the excited $^2F_{5/2}$ state to conserve the residual energy giving rise to Yb^{3+} infrared luminescence.[19] However, the probability that the Yb^{3+} returns in the excited state after electron back-transfer is small, since the intensity of sensitized luminescence is rather weak in our borate glasses. This is analogous to the results obtained in $Y_3Al_5O_{12}$ ceramics.[5]

C. Generalization of electron transfer mechanism using VRBE scheme

So far, the electron transfer mechanism satisfactorily explains the Ce^{3+} luminescence quenching in Yb^{3+} codoped

materials. A similar electron transfer mechanism has also been reported in Ce^{3+}-Eu^{3+} [18] and Pr^{3+}-Eu^{3+} (Ref. 27) ion pairs. This can be understood from the Dorenbos model on the absolute electron binding energies in lanthanide levels, which predicts the possibility of electron transfer mechanism between rare earth ions.[22–24] Figure 9 shows the vacuum referred electron binding energy (VRBE) scheme for the trivalent and the di-valent lanthanide ions in the studied glass. It is based on the following relation:[24]

$$E_{4f}(7,2+,A) = -24.92 + \frac{18.05 - U(6,A)}{0.777 - 0.0353U(6,A)}, \quad (1)$$

where $E_{4f}(7,2+,A)$ is the vacuum referred binding energy (VRBE) of an electron in the $4f^7$ ground state of Eu^{2+} ions in the chemical environment A. $U(6,A)$ is the Coulomb repulsion energy, which is useful to estimate the chemical shift due to the environment A with respect to the binding energy in free Eu^{2+} ion ground state (−24.92 eV). The Coulomb repulsion energy, $U(6,A)$ was estimated from the centroid shift (ε_c) of the Ce^{3+}: 4f → $5d_j$ transitions using the following relation and is found to be 7.05 ± 0.01 eV (Ref. 24)

$$U(6,A) = 5.44 + 2.83\exp\left[\frac{-\varepsilon_c(1,3+,A)}{2.2}\right] \quad (2)$$

The centroid shift was calculated to be 1.25 ± 0.01 eV in the studied glasses. Based on the above calculations, the VRBE of Eu^{2+} ground state electron, E_{4f} (7,2+,A) is found to be −4.09 ± 0.01 eV. The $U(6,A)$ represents the energy difference between Eu^{2+} and Eu^{3+} ground state, and therefore by knowing this, the VRBE diagram for entire lanthanide family can be constructed using the chemical shift model as suggested by Dorenbos.[22,28] The Eu^{3+} CT energy (5.4 ± 0.1 eV) is used for locating the valence band position in the VRBE scheme. Note that the only relevant parameters for predicting electron transfer possibilities in the VRBE scheme of Fig. 9 are $U(6,A)$ and the energy of the first excitation transition of donor ion (4f → $5d_1$ in case of Ce^{3+}). Errors in the band gap value and the CT-band energy of Eu^{3+}, Yb^{3+}, or Ce^{4+} used to place the valence band and conduction band are not relevant. Even with an error of ±0.1 eV in $U(6,A)$ the conclusions in this work remain the same.

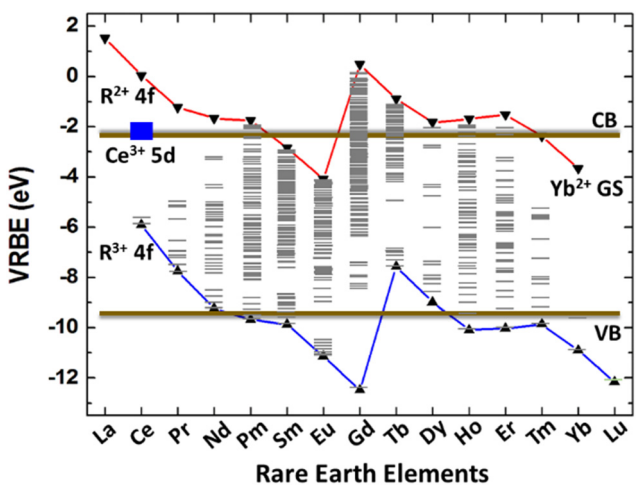

FIG. 9. VRBE scheme of di-valent and tri-valent lanthanide ions in borate glass.

From the VRBE scheme in Fig. 9, it can be seen that the binding energy in the Yb^{2+} ground state is at lower energy than in the Ce^{3+} $5d_1$ state, which therefore allows the electron transfer from Ce^{3+} to Yb^{3+} ions as discussed in earlier section. Similarly, the electron transfer is favored among Ce^{3+}-Eu^{3+} pairs, where the binding energy in the excited $5d_1$ state of Ce^{3+} is usually at higher energy than that in the Eu^{2+} ground state.[18] This electron transfer mechanism may be responsible for the poor luminescence performance in Ce^{3+}-Eu^{3+} codoped system over the Ce^{3+}-Tb^{3+} system.[29] From Fig. 9, it is possible to understand the electron transfer mechanism among other opposite oxidation/reduction property rare earth ions. The only condition is that the electron transfer should be energetically favorable. In case of Tb^{3+}-Yb^{3+} codoped materials, Tb^{3+} shows more quenching under $^5D_3$ excitation (~380 nm) than under $^5D_4$ state excitation (~480).[30,31] This was explained by Ueda and Tanabe, suggesting the presence of electron transfer mechanism from the $^5D_3$ state of Tb^{3+} to Yb^{3+} ions, whereas the phonon assisted electric dipole-dipole interactions under the low energy $^5D_4$ excitation.[30] This can be understood from the VRBE diagram in Fig. 9, which shows that the electron binding energy in the $^5D_3$ state of Tb^{3+} is close to that in the Yb^{2+} ground state energy allowing for electron transfer interactions; whereas, the $^5D_4$ state is at significantly lower energy making electron transfer energetically forbidden. Similarly, in case of the Eu^{2+}-Yb^{3+} pair, the electron binding energy of the Eu^{2+} 5d state is higher than the Yb^{2+} ground state as per the VRBE scheme, thus making it energetically more favorable for the electron transfer mechanism over the quantum cutting mechanism.

V. CONCLUSION

In summary, a detailed investigation on Ce^{3+} sensitized Yb^{3+} infrared luminescence has been carried out in the studied borate glass. The Ce^{3+} PL and decay lifetime have shown strong quenching in presence of Yb^{3+} codoping in the glasses. However, the intensity of sensitized Yb^{3+} luminescence has observed to be very poor. Similarly, the absolute luminescence quantum yield also showed a decrease in codoped glasses, which strongly contradicts with the quantum cutting or the cooperative energy transfer mechanism. On the contrary, we conclude that the electron transfer mechanism is more favorable in Ce^{3+}-Yb^{3+} pair, which has successfully been explained with the help of host referred and vacuum referred binding energy schemes of the electrons in Ce^{3+} and Yb^{3+} ions. A generalized model for predicting the electron transfer mechanism among different opposite oxidation/reduction property dopant ions has been presented based on the vacuum referred electron binding energy scheme of lanthanide ions and explained in detail. Accordingly, the electron transfer mechanism is energetically more favorable in many dopant pairs such as the Ce^{3+}-Yb^{3+}, Ce^{3+}-Eu^{3+}, Eu^{2+}-Yb^{3+}, etc., over the quantum cutting or the other related mechanisms.

ACKNOWLEDGMENTS

This work was carried out under the JSPS Post-Doctoral Fellowship program (P13372).

[1]R. Reisfeld and S. Neuman, Nature **274**, 144 (1978).
[2]M. J. Currie, J. K. Mapel, T. D. Heidel, S. Goffri, and M. A. Baldo, Science **321**, 226 (2008).
[3]F. Purcell-Milton and Y. K. Gun'ko, J. Mater. Chem. **22**, 16687 (2012).
[4]W. Shockley and H. J. Queisser, J. Appl. Phys. **32**, 510 (1961).
[5]J. Ueda and S. Tanabe, J. Appl. Phys. **106**, 043101 (2009).
[6]R. T. Wegh, H. Donker, K. D. Oskam, and A. Meijerink, Science **283**, 663 (1999).
[7]J. L. Sommerdijk, A. Bril, and A. W. de Jager, J. Lumin. **8**, 341 (1974).
[8]R. T. Wegh, E. V. D. Van Loaf, and A. Meijerink, J. Lumin. **90**, 111 (2000).
[9]D. Serrano, A. Braud, J. L. Doualan, W. Bolaños, R. Moncorgé, and P. Camy, Phys. Rev. B **88**, 205144 (2013).
[10]X. Huang, S. Han, W. Huang, and X. Liu, Chem. Soc. Rev. **42**, 173 (2013).
[11]Q. Duan, F. Qin, Z. Zhang, and W. Cao, Opt. Lett. **37**, 521 (2012).
[12]D. Timmerman, I. Izeddin, P. Stallinga, I. N. Yassievich, and T. Gregorkiewicz, Nature Photon. **2**, 105 (2008).
[13]Q. Yan, J. Ren, Y. Tong, and G. Chen, J. Am. Ceram. Soc. **96**, 1349 (2013).
[14]D. Chen, Y. Wang, Y. Yu, P. Huang, and F. Weng, J. Appl. Phys. **104**, 116105 (2008).
[15]A. Baccolini, J. Marcues-Heuso, D. Chen, Y. Wang, and B. S. Richards, Sol. Energy Mater. Sol. Cells **122**, 8 (2014).
[16]Z. Liu, J. Li, L. Yang, Q. Chen, Y. Chu, and N. Dai, Sol. Energy Mater. Sol. Cells **122**, 46 (2014).
[17]Z. Fang, R. Cao, F. Zhang, Z. Ma, G. Dong, and J. Qiu, J. Mater. Chem. C **2**, 2204 (2014).
[18]A. A. Setlur and J. J. Shiang, J. Phys. Chem. C **114**, 2792 (2010).
[19]F. You, A. J. J. Bos, Q. Shi, and P. Dorenbos, J. Phys.: Condens. Matter **23**, 215502 (2011).
[20]A. D. Sontakke and K. Annapurna, J. Lumin. **138**, 229 (2013).
[21]P. Vergeer, T. J. H. Vlugt, M. H. F. Kox, M. I. den Hertog, J. P. J. M. van der Eerden, and A. Meijerink, Phys. Rev. B **71**, 014119 (2005).
[22]P. Dorenbos, J. Mater. Chem. **22**, 22344 (2012).
[23]P. Dorenbos, J. Phys.: Condens. Matter **15**, 8417 (2003).
[24]P. Dorenbos, J. Lumin. **135**, 93 (2013).
[25]J. Ueda, S. Tanabe, and T. Nakanishi, J. Appl. Phys. **110**, 053102 (2011).
[26]E. van der Kolk, O. M. Ten Kate, J. W. Wiegman, D. Biner, and K. W. Krämer, Opt. Mater. **33**, 1024 (2011).
[27]P. Vergeer, V. Babin, and A. Meijerink, J. Lumin. **114**, 267 (2005).
[28]P. Dorenbos, ECS J. Solid State Sci. Technol. **3**, R19 (2013).
[29]C. Ma, S. Jiang, and X. Zhou, J. Rare Earths **28**, 40 (2010).
[30]J. Ueda and S. Tanabe, Phys. Status Solidi A **208**, 1827 (2011).
[31]S. Ye, Y. Katayama, and S. Tanabe, J. Non-Crystal. Solids **357**, 2268 (2011).